iScience, Volume *26*

Supplemental information

A proton-inhibited DEG/ENaC ion channel maintains neuronal ionstasis and promotes neuronal survival under stress

Dionysia Petratou, Martha Gjikolaj, Eva Kaulich, William Schafer, and Nektarios Tavernarakis

Supplemental Figures

Figure S1

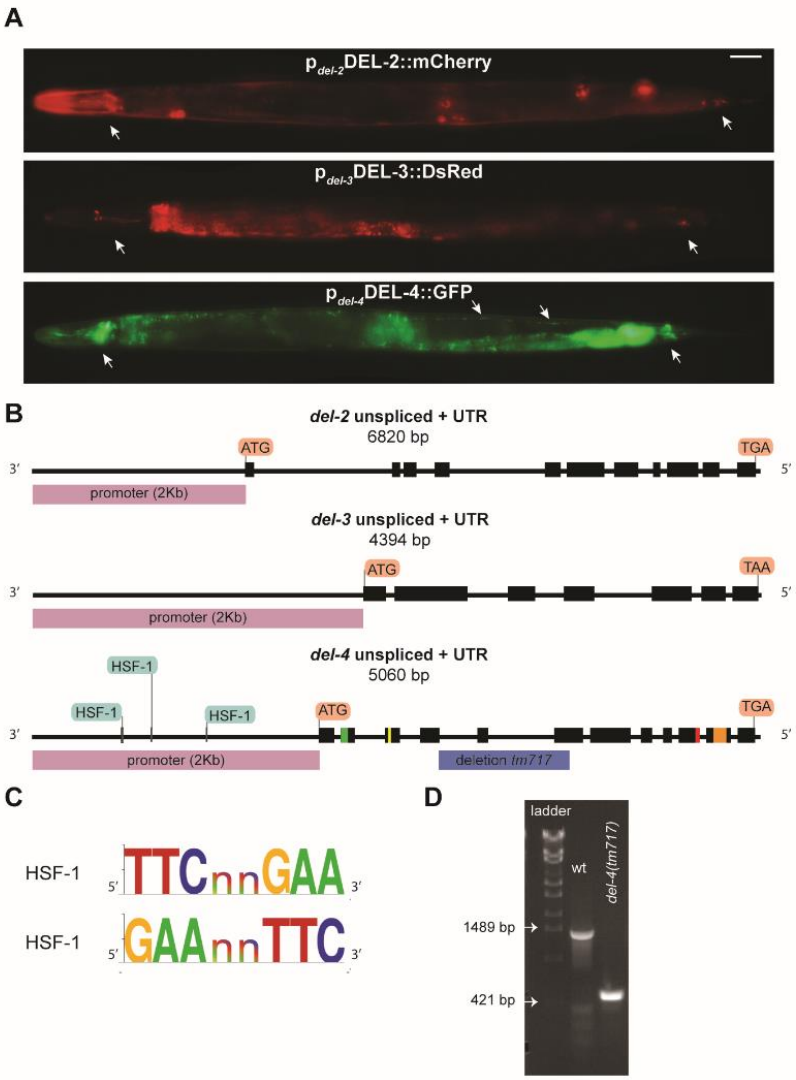

Figure S2

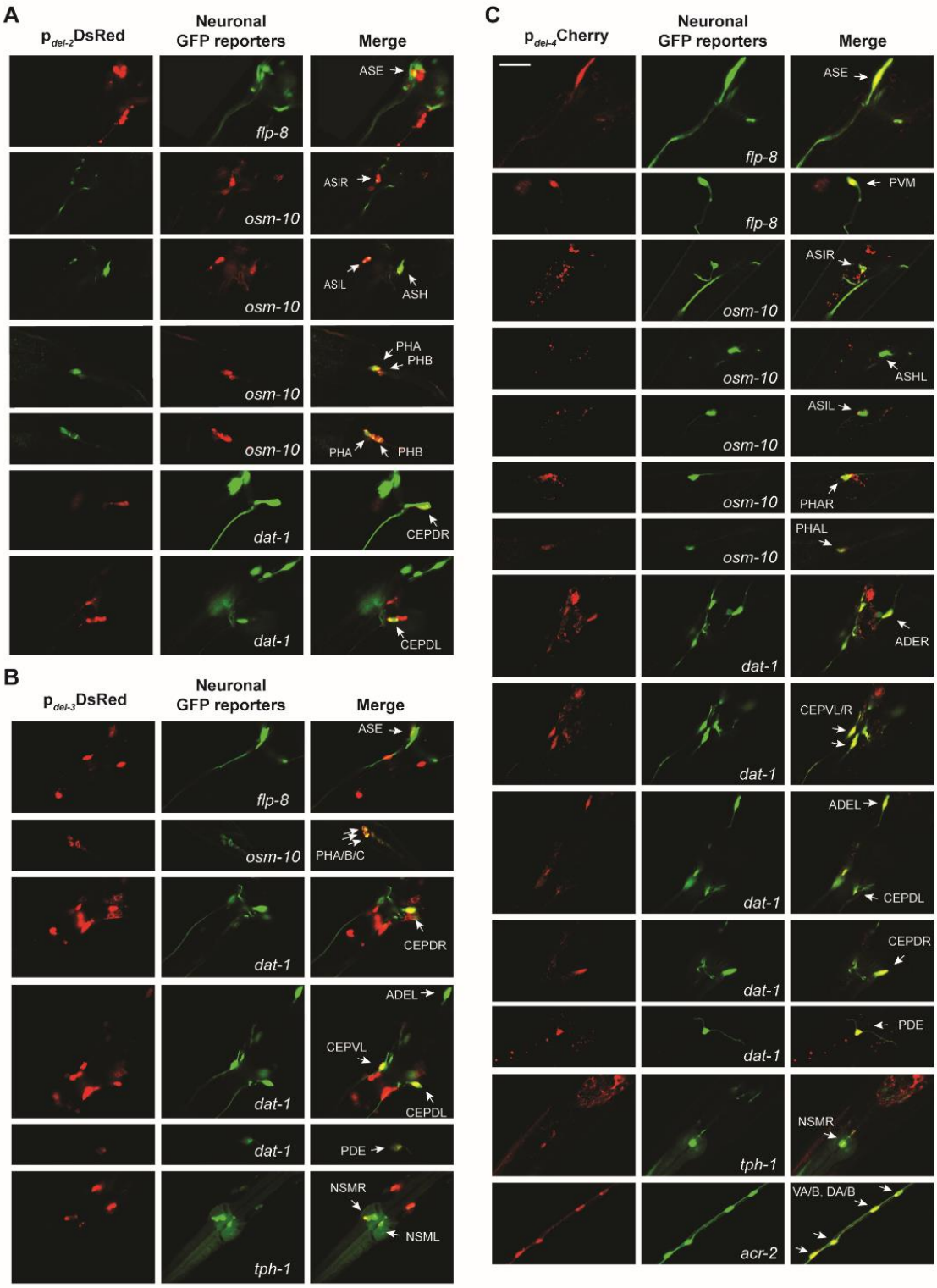
A
p del-2 DsRed
Neuronal GFP reporters
Merge
ASE
flp-8
ASIR
osm-10
ASIL
ASH
PHA
PHB
dat-1
CEPDR
CEPDL
B
p del-3 DsRed
PHA/B/C
ADEL
CEPVL
PDE
tph-1
NSMR
NSML
C
p del-4 Cherry
PVM
ASHL
PHAR
PHAL
CEPVL/R
acr-2
VA/B, DA/B

Figure S3

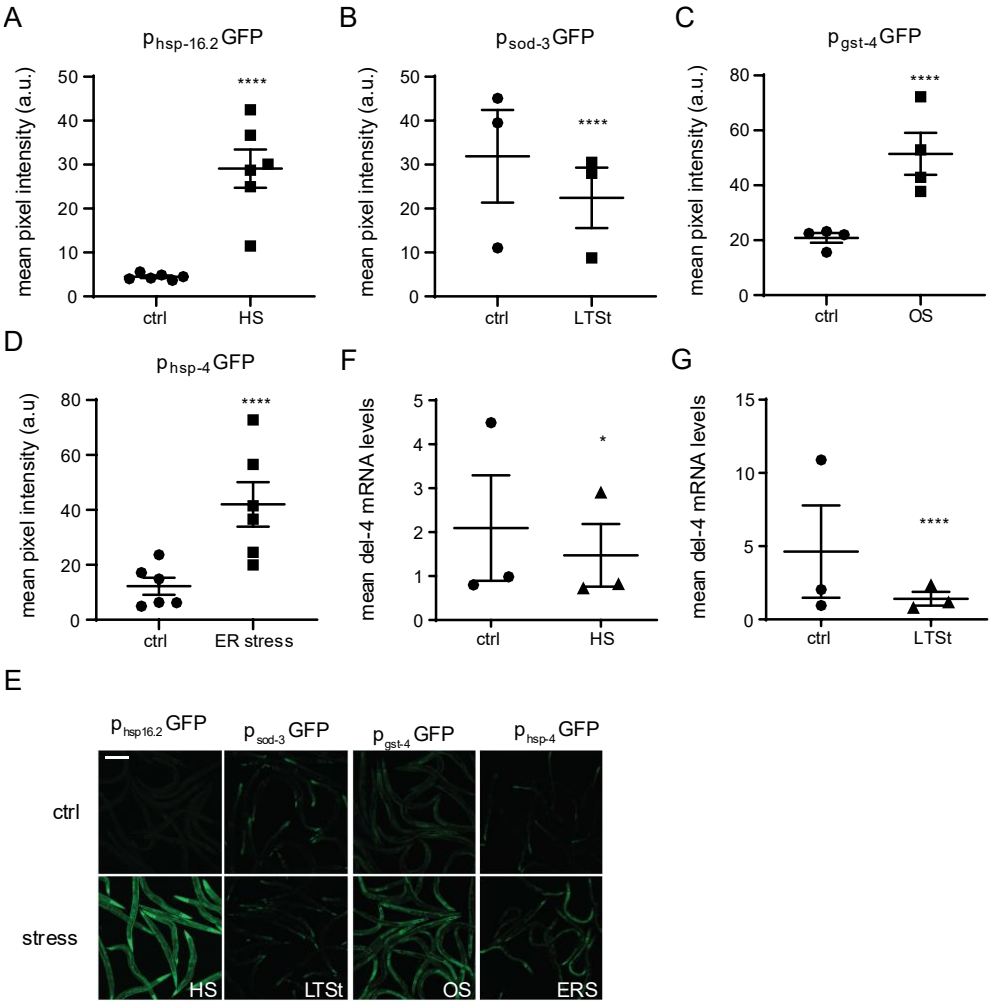
A
p hsp-16.2 GFP
mean pixel intensity (a.u.)
50
40
30
20
10
0
****
ctrl
HS
B
p sod-3 GFP
mean pixel intensity (a.u.)
50
40
30
20
10
0
****
ctrl
LTSt
C
p gst-4 GFP
mean pixel intensity (a.u.)
80
60
40
20
0
****
ctrl
OS
D
p hsp-4 GFP
mean pixel intensity (a.u)
80
60
40
20
0
****
ctrl
ER stress
F
mean del-4 mRNA levels
5
4
3
2
1
0
*
ctrl
HS
G
mean del-4 mRNA levels
15
10
5
0
****
ctrl
LTSt
E
p hsp16.2 GFP
p sod-3 GFP
p gst-4 GFP
p hsp-4 GFP
ctrl
stress
HS
LTSt
OS
ERS

Figure S4

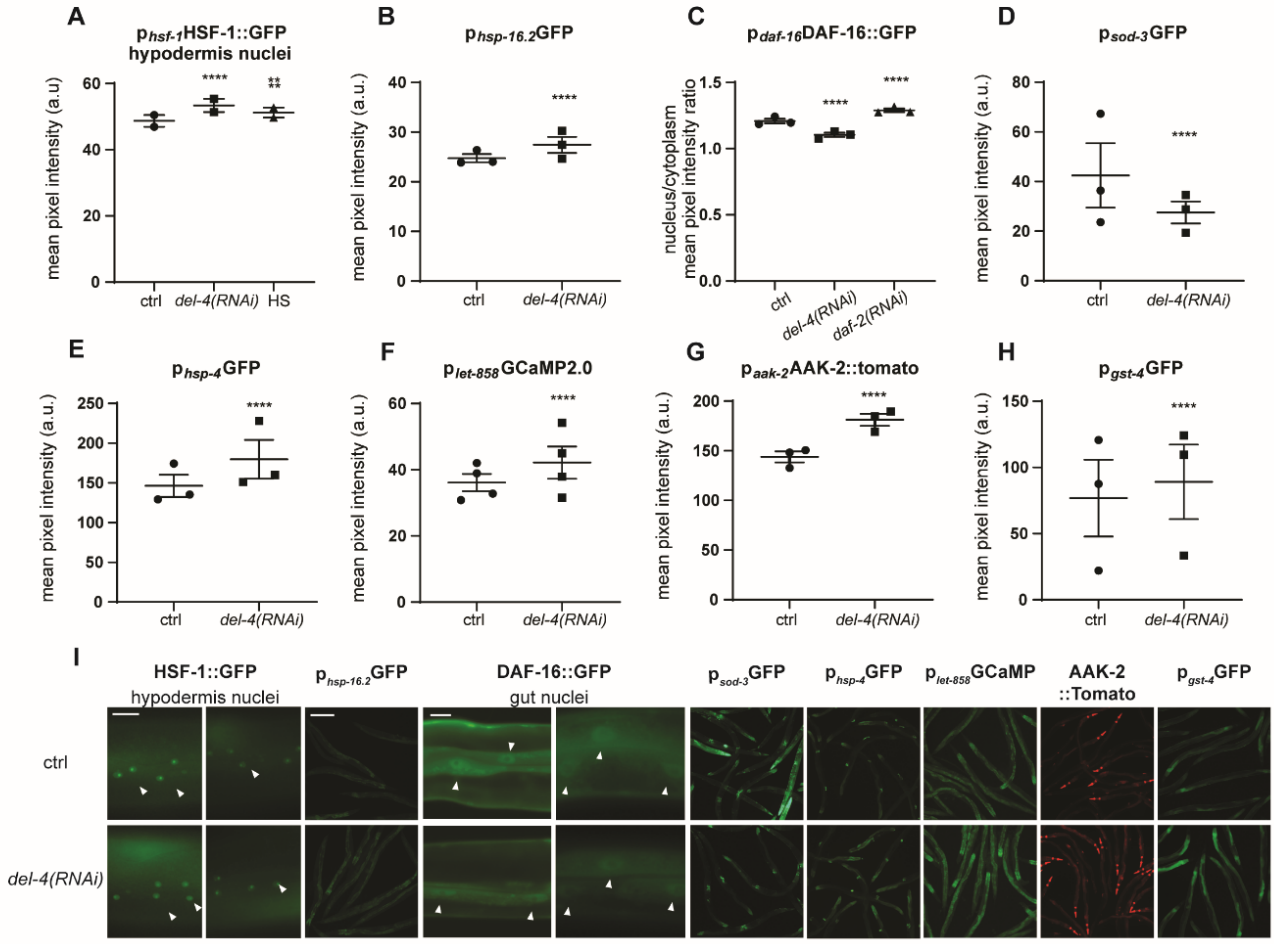
A
phsf-1HSF-1::GFP
hypodermis nuclei
mean pixel intensity (a.u)
ctrl
del-4(RNAi)
HS
B
phsp-16.2GFP
mean pixel intensity (a.u.)
ctrl
del-4(RNAi)
C
pdaf-16DAF-16::GFP
nucleus/cytoplasm
mean pixel intensity ratio
ctrl
del-4(RNAi)
daf-2(RNAi)
D
psod-3GFP
mean pixel intensity (a.u.)
ctrl
del-4(RNAi)
E
phsp-4GFP
mean pixel intensity (a.u.)
ctrl
del-4(RNAi)
F
plet-858GCaMP2.0
mean pixel intensity (a.u.)
ctrl
del-4(RNAi)
G
paak-2AAK-2::tomato
mean pixel intensity (a.u.)
ctrl
del-4(RNAi)
H
pgst-4GFP
mean pixel intensity (a.u.)
ctrl
del-4(RNAi)
I
HSF-1::GFP
hypodermis nuclei
phsp-16.2GFP
DAF-16::GFP
gut nuclei
psod-3GFP
phsp-4GFP
plet-858GCaMP
AAK-2
::Tomato
pgst-4GFP
ctrl
del-4(RNAi)

Figure S5

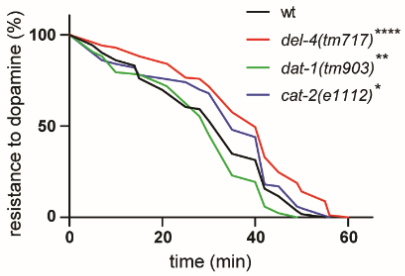

Figure S6

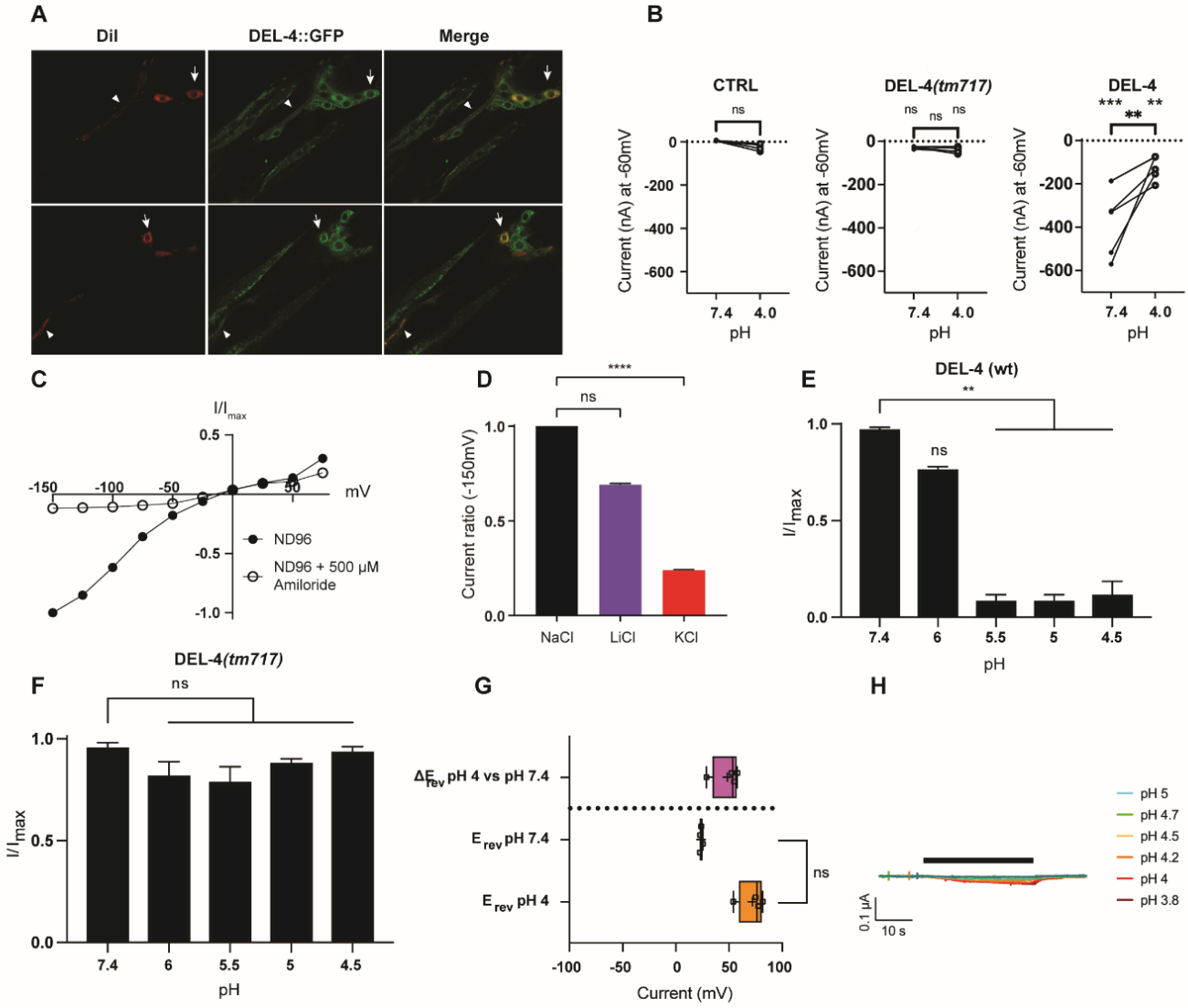

Supplemental Figure Legends

Figure S1. Expression pattern and gene structure of *del-2*, *del-3* and *del-4*, Related to Figures 1 and 2.

(A) All three DELs are expressed in neuronal cells of the head and tail of *C. elegans*. In addition, DEL-4 localizes to a series of neurons along the *C. elegans* body. Epifluorescence images of lines expressing the *del-2*, *del-3* and *del-4* translational reporters. Arrows indicate sites of expression. Lens 20x. We captured images from the head, midbody, and tail regions and aligned them using Adobe Photoshop CS5 to illustrate the entire animal. Left is anterior. Scale bar 50 μm.

(B) Genetic loci of *del-2*, *del-3* and *del-4* genes. Black boxes, starting from ATG until the stop codon, indicate the exons. Upstream of ATG is designated the 2 kb of the promoter region (pink box) and binding sites of HSF-1 transcription factor in the *del-4* promoter (cyan boxes). Site of deletion identified in the *del-4(tm717)* mutant is indicated with blue box below the *del-4* open reading frame. The deletion site in the *del-4* gene induce the development of premature stop codon immediately after the missing sequence. Representation of coding regions that correspond to protein domains is shown in green, yellow, red, and orange, respectively. The green region represents the first transmembrane domain, the yellow box denotes the post-M1 domain, the red region corresponds to the pre-M2 domain and the orange box denotes the second transmembrane domain. The region between the two transmembrane domains corresponds to the extracellular domain. We retrieved the DNA sequences and exon/intron annotations from WormBase (https://wormbase.org//). We utilized the bioinformatics tool Phobius (https://phobius.sbc.su.se/) (see KRT) to estimate the transmembrane domains. Annotation of the *del-2* sequence corresponded to that of isoform 1. Transcription factor binding sites in the promoter region of *del-4* correspond only to the forward direction. We employed the software product SnapGene (KRT) for editing and annotating the DNA sequences.

(C) DNA sequences previously identified as HSF-1 binding sites (1). To generate DNA sequence logos, we used the WEBLOGO application (https://weblogo.berkeley.edu/) (2). Letter n represents any nucleotide.

(D) Agarose gel electrophoresis image of PCR products for the *del-4 gene*, using as template genomic DNA isolated from wt and *del-4(tm717)* mutant animals. We used 1% w/v agarose gel

stained with ethidium bromide. We used primers flanking the DNA region *del-4* mutations to amplify the genomic DNA. Predicted band sizes: wt 1404 bp, *del-4(tm717)* 498 bp. We generated the ladder by digesting λ phage DNA with StyI.

Figure S2. Neuronal expression of DEL-2, DEL-3 and DEL-4, Related to Figure 1.

(A) Expression pattern of DEL-2 in chemosensory and dopaminergic neurons (ASE, ASH, ASI, PHA, PHB, and CEPDL/R) (Tables S2 and S3).

(B) DEL-3 expression in chemosensory, dopaminergic, and serotonergic neurons (ASE, PHA, PHB, PHC, CEPDL/R, CEPVL, ADEL, PDE, and NSMR/L) (Tables S2 and S3).

(C) Localization of DEL-4 in amphid, phasmid, dopaminergic, serotonergic, mechanosensory and cholinergic motor neurons (ASE, ASI, ASH and PHA, PVM, CEPDL/R, CEPVL/R, ADEL/R, PDE, NSMR, VA/B, DA/B) (Tables S2 and S3).

(A-C) Confocal images (Z-stacks) of strains co-expressing mCherry or DsRed under the *del-2, del-3* or *del-4* promoters (left in each panel seen in red) and GFP driven by *flp-8*, *osm-10*, *dat-1*, *tph-1* or *acr-2* promoters (middle seen with green). Promoters of *flp-8* and *osm-10* drive expression in the sensory neurons, ASE, URX, PVM and ASH, ASI, PHA, PHB, respectively. The promoter of *dat-1* drives the expression of GFP in the dopaminergic neurons (CEPD, CEPV, ADE, PDE), the *tph-1* promoter in the serotonergic neurons (NSM, ADF) and the *acr-2* promoter in the cholinergic motor neurons (VA/B, DA/B. (right) The right column of each panel corresponds to merged images. We utilized merged images of z-stacks to assess colocalization. One day adult animals**.** Arrows indicate neuronal cell somas where mCherry or DsRed is co-expressed with GFP. Lens 40x. Left is anterior. Scale bar 20 μM.

Figure S3. Control experiments for stress-induction assays, Related to Figure 2.

(A) Heat stress for 2.5 hrs at 37 °C and O/N recovery induces the expression of the heat shock chaperone HSP-16.2. We measured the fluorescence intensity from the whole body of animals expressing the transcriptional reporter $p_{hsp\text{-}16.2}$GFP upon control temperature (20 ^{o}C) and HS.

(B) Long-term starvation for 24 hrs reduces SOD-3 expression levels. The mean fluorescence intensity was measured from the whole body of well-fed and starved animals expressing the $p_{sod\text{-}3}$GFP transcriptional reporter.

(A, B) We applied stress on day one of adulthood and imaged the animals on day two.

(C) Induction of GST-4 expression after treatment for 24 hrs with paraquat plated on OP50-seeded NGM plates to a final concentration of 8 mM. We measured the expression levels of GST-4 from the whole body of animals expressing the p_{gst-4}GFP transcriptional reporter, upon control conditions and oxidative stress.

(D) HSP-4 expression levels increase after 24 hrs of treatment with 5 μg/ml tunicamycin plated on OP50-seeded NGM plates. We used animals expressing the transcriptional reporter p_{hsp-4}GFP and measured mean fluorescence intensity from the entire animal.

(C, D) We placed animals at the L4 stage on paraquat or tunicamycin and imaged them on day one of adulthood.

(F, G) Reduced *del-4* mRNA levels upon HS and LTSt. We measured with RT-PCR the mean *del-4* mRNA levels, using as template cDNA from 2-day adult wt animals upon control conditions, HS and LTSt. We isolated total mRNA from wt animals (control and stressed, reversely transcribed it into complementary DNA (cDNA) and used it as template for RT-PCR. Dot plot, dots represent the mean *del-4* mRNA levels from independent biological replicates. We performed 3 independent biological replicates and for each biological we performed three technical replicates.

(E) Representative images of indicated reporters upon control and stress conditions. 5x lens. Scale bar 200 μm.

(A-D) Dot plots, dots represent the mean fluorescence of independent biological replicates. n represents the number of animals.

(F-G) Dot plots, dots represent the mean mRNA levels of independent biological replicates.

(A-D, F,G) Error bars represent SEM. ns p=0.1234, *p=0.0332, **p=0.0021, ***p=0.0002, ****p<0.0001. Two-way ANOVA analysis.

(A) ctrl n=141, HS n=119, (B) ctrl n=110, LTSt n=80, (C) ctrl n=103, OS n=80, (D) ctrl n=57, ERS n=62.

Figure S4. DEL-4 deficiency interferes with activation of distinct stress responses

Related to Figure 3.

(A) HSF-1 expression levels in hypodermis nuclei increased upon *del-4(RNAi)*. We measured the mean fluorescence intensity of hypodermis nuclei of animals expressing the p_{hsf-1}HSF-1::GFP construct. We overlooked the nuclei located above the gut to avoid intestinal autofluorescence. The expression levels of HSF-1 upon HS treatment served as the positive control.

(B) Depletion of *del-4* with RNAi increases the expression levels of the HSF-1 target HSP-16.2. We used the $p_{hsp-16.2}$GFP transcriptional reporter expressing animals and measured the whole body upon control and *del-4(RNAi)* conditions.

(C) The DAF-16 ratio of the nucleus to the cytoplasm decreased upon *del-4(RNAi)*. *daf-2* RNAi was used as a positive control. We measured the intensity levels of DAF-16 in the nuclei and adjacent cytoplasm of the gut, using a strain expressing the p_{daf-16}DAF-16::GFP translational reporter.

(D) Elimination of *del-4* with RNAi lowers the expression levels of the DAF-16 target SOD-3. We measured the fluorescence intensity from the whole body of 4-day adult animals expressing the p_{sod-3}GFP transcriptional reporter upon control and *del-4* RNAi conditions.

(E) Depletion of *del-4* with RNAi increases the expression levels of HSP-4, an ER stress marker. We used animals expressing the transcriptional reporter p_{hsp-4}GFP and measured fluorescence intensity from the whole body upon control and *del-4(RNAi)* conditions.

(F) Cytoplasmic Ca^{2+} levels rise upon *del-4(RNAi)*. Measurement of intracellular Ca^{2+} levels using animals expressing the genetically encoded calcium indicator GCaMP2.0 driven by the *let-858* promoter for systemic expression. Measurments were obtained from the whole body.

(G) Increased AAK-2 expression levels were observed upon *del-4(RNAi)*. We measured mean fluorescence intensity from the whole body of animals expressing the translational reporter p_{aak-2}AAK-2::Tomato.

(H) The expression level of the SKN-1 target GST-4 increase upon treatment with *del-4(RNAi)*. The expression levels of animals expressing the transcriptional reporter p_{gst-4}GFP were measured from the whole body.

(I) Representative images of the designated reporters. Scale bars, 20 μm apart from the images corresponding to P_{hsf-1}HSF-1::GFP (hypodermis nuclei) and DAF-16::GFP (gut nuclei), where the scale bar corresponds to 200 μm. P_{hsf-1}HSF-1::GFP (hypodermis nuclei): 40x lens, DAF-16::GFP (gut nuclei): 20x, rest of the images: 5x lens. Left is anterior

(A-D, F, H) Four-day adult animals. (E, G) 3-day adult animals.

(A-H) Dot plots, dots represent the mean fluorescence intensity of independent biological replicates. Error bars represent SEM. ns p=0.1234, *p=0.0332, **p=0.0021, ***p=0.0002, ****p<0.0001. Two-way ANOVA analysis. (A) ctrl n= 257, *del-4(RNAi)* n=291, HS n=392, n = the number of hypodermis nuclei measured. (B) ctrl n=245, *del-4(RNAi)* n=177. (C) ctrl n=519, *del-4(RNAi)* n=733, daf-2(RNAi) n=642, n = the number of gut nuclei measured. (D) ctrl n=156, *del-4(RNAi)* n=154. (E) ctrl n=128, *del-4(RNAi)* n=154. (F) ctrl n=207, *del-4(RNAi)* n=217, (G) ctrl n=142, *del-4(RNAi)* n=127, (H) ctrl n=250, *del-4(RNAi)* n=245.

Figure S5. Animals lacking DEL-4 are resistant to exogenously applied dopamine, Related to Figure 5.

DEL-4 amelioration results in increased resistance to dopamine. We measured the time to paralysis in a 20 μl drop of 40 mM dopamine of ctrl, *del-4(tm717)*, *dat-1(tm903)* and *cat-2(e1112)* animals (Tables 1 and S4). *dat-1(tm903)* and *cat-2(e1112)* animals were used as controls. *dat-1* encodes for the dopamine transporter; thus, in the absence of DAT-1 dopamine is retrieved from the synapse back to the pro-synaptic cell accumulating at the synaptic cleft. Therefore, dat-1 mutants are expected to paralyze faster compared to wt. CAT-2 is involved in dopamine biosynthesis from tyrosine. Therefore, in the absence of CAT-2 reduced amount of dopamine would be released at the synaptic cleft and it would take more time for *cat-2* mutants to paralyze in dopamine compared to wt. We observed that *del-4* and *cat-2* mutant animals are resistant to dopamine, while *dat-1(tm903)* animals are sensitive. Experiments were performed with day-1 adult animals. Survival curve analysis was performed for estimation of significance. ns p=0.1234, *p=0.0332, **p=0.0021, ***p=0.0002, ****p<0.0001. Ctrl n=172, *del-4(tm717)* n=170, *dat-1(tm903)* n=170, *cat-2(31112)* n=100. n represents number of animals.

Figure S6. Amiloride and low pH block the homomeric DEL-4 sodium channel, Related to Figures 6 and 7.

(A) Membranous localization of DEL-4 on neuronal cells. Confocal images show the colocalization of GFP expression with the lipophilic dye DiI at the surface of neuronal cell bodies and processes, examined on animals expressing the p_{del-4}DEL-4::GFP translational reporter and stained with DiI. Left, p_{del-4}DEL-4::GFP expressing animals (green). Middle, DiI staining in Red. Right, merged images. We utilized merged images of z-stacks to assess colocalization. Neuronal cell bodies (arrows) and dendrites (small arrowheads) are indicated. Left is anterior. One day adult animals**.** Scale bar 20 μM. Confocal images (Z-stacks) at 63x lens.

(B) DEL-4 currents at neutral pH are inhibited at pH 4. Currents of the nuclease-free water-injected controls and the truncated DEL-4(tm717) mutant currents are not blocked by acidic pH 4. Graphs show raw current upon perfusion with either pH 7.4 (filled circle) or pH 4 (open circle) as indicated, for *Xenopus* oocytes injected with the DEL-4 *wild-type* or *tm717* mutant, or water-injected controls. Lines connect data from individual oocytes. (n = (from left to right) 5, 5, 6) Currents were recorded at a holding potential of -60mV.

(C) Amiloride inhibits the DEL-4 channel. Current-voltage (I-V) relationships for *Xenopus* oocytes injected with *del-4* cRNA, following perfusion of oocytes with a physiological NaCl solution (1X ND96) (black circles), and in the presence of 500 μM of the DEG/ENaC channel blocker amiloride (open circles) (n = 10). Voltage steps were from – 150 mV to +75 mV, from a holding potential of -60 mV.

(D) The DEL-4 channel is permeable to monovalent cations (Na^+, Li^+), as established by determining the ratio of the current at -150 mV when perfusing oocytes with NaCl, LiCl or KCl solutions (n = 10).

(E-F) Low pH in the range of 4.5-5.5 blocks the DEL-4 homomeric channel. Heterologously expressed DEL-4 channel, perfused with solutions of increasing pH starting from pH 4.5 to 7.5 (n = 5). Currents were recorded at a holding potential of -60mV, normalized to maximal currents (I/I_{max}), Kruskal-Wallis test and post-hoc Dunnett's multiple comparisons test found no significant difference in current ratio for the DEL-4(*tm717*) mutant controls, but DEL-4 wild-type currents were significantly blocked at low pH (n = 5 each). Amount of total cRNA (500 ng/μl) injected for each construct. Error bars represent Mean and SEM.

(G) DEL-4 ins not permeable for protons. Summary of reversal potential E_{rev} of DEL-4 expressing oocytes and controls (DEL-4(tm717) mutant and water-injected oocytes) when perfused with basal pH 7.4 (cyan) and acidic pH 4 (orange) (top to bottom, n= 6, 8, 3). Low pH did not statistically significantly change the E_{rev} as assessed by a paired Wilcoxon test (top to bottom, p=0.094, ns; p=0.844, ns; p =0.750, ns). DEL-4(tm7171) and water-injected controls have significantly lower currents which might contribute to higher variability. Data are presented as boxplots with median (dash), mean (cross) and min and max error bars. E_{rev} were calculated as described in Star methods.

(H) Representative traces of water-injected *Xenopus* oocytes used as controls of DEL-4 expressing oocytes when perfused with ND96 solution at various proton concentrations from a neutral baseline (pH 7.4). Currents were recorded at a holding potential of -60mV, and traces were baseline-subtracted and drift-corrected using Roboocyte2+ (Multichannels) software.

References

1. Trinklein ND, Murray JI, Hartman SJ, Botstein D, Myers RM. The role of heat shock transcription factor 1 in the genome-wide regulation of the mammalian heat shock response. Mol Biol Cell. 2004;15(3):1254-61.
2. Crooks GE, Hon G, Chandonia JM, Brenner SE. WebLogo: a sequence logo generator. Genome Res. 2004;14(6):1188-90.

Supplemental Tables

Table S1. List of abbreviations used in the paper, Related to Star methods.

Abbreviation	Definition
a.u.	arbitrary units
ACh	Acetylcholine
AD	Alzheimer's Disease
ALS	Amyotrophic Lateral Sclerosis
AMP	Adenosine MonoPhosphate
AMPK	AMP-activated protein Kinase
ANOVA	one-way ANalysis Of Variance
AS	Acidic Stress
ASAP1	Accelerated Sensor of Action Potentials1 (Genetic Voltage Indicator)
ASICs	Acid Sensing sodium Channels
BLAST	Basic Local Alignment Search Tool
BS	Basal Slowing
BSA	Bovine Serum Albumin
BSR	Basal Slowing Response
BSRC	Biomedical Sciences Research Center
CaMKK2	Calcium/CalModulin-dependent protein Kinase Kinase 2
cAMP	cyclic Adenosine MonoPhosphate
cRNA	coplementary RNA
ctrl	control
DCVs	Dense Core Vesicles
DEG	DEGenerin
DEL	DEgenerin Like
DiI	Dioctadecyl tetramethylIndodicarbocyanine-disulphonic acid, lipophilic carbocyanine tracer
ds RNA	double stranded RNA
DsRED	Red fluorescent protein from Discosoma
EGFP	enhanced GFP
ENaC	Epithelial sodium (Na^+) Channel
ER	Endoplasmic Reticulum
ERC	European Research Council
E_{rev}	average reversal potential
ERS	ER Stress
ER^{UPR}	ER Unfolded Protein Response
ESF	European Social Fund
FOXO	FOrkhead boX O4
GABA	Gamma-AminoButyric Acid
GCaMP2.0	Genetically encoded CalciuM indicator 2.0

GFP	Green Fluorescent Protein
HB101	*Eserichia coli* bacterial strain
HEPES	(4-(2-HydroxyEthyl)-1-PiperazineEthanesulfonic acid), a zwitterionic sulfonic acid buffering agent
hr/hrs	hour/hours
HS	Heat Stress
HSF1	Heat Shock transcription Factor 1
HSPs	Heat Shock Proteins
HT115(DE3)	*Eserichia coli* bacterial strain, commonly used for gene knockdown with RNAi
I	current
IC50	half-maximal inhibitory concentration
Imax	maximal current
IQD	interquartile range
IV	Current-voltage relationships
kb	kilobase
KCNQ	voltage-gated potassium channel
KRT	Key Resources Table
L4 stage	Larval stage 4
LTSt	Long-Term Starvation
M13	isotonic buffer solution for *C. elegans*
M9	isotonic buffer solution for *C. elegans*
mCherry	a member of the mFruits family of monomeric red fluorescent proteins
MES	2-(N-Morpholino)EthaneSulfonic acid
mg	milligram
ml	millilitre
mM	millimolar
mRNA	messenger RNA
mV	milliVolt
N2	*C. elegans* wild type isolate, Bristol variation
NCBI	National Center for Biotechnology Information
NCRR	National Center for Research Resources
ND96	physiological NaCl solution
NEB	New England Biolabs
ng	nanogram
NGM	nematode growth medium
NIH	National Institutes of Health
NLS	Nuclear Localization Signal
NMJ	Neuromuscular Junction
NRF2	Nuclear Factor erythroid 2 - related factor 2
NSRF	National Strategic Reference Framework
O/D	Over Day
O/N	Over Night
OP50	Eserichia coli bacterial strain, common *C. elegans* food source in the laboratory

OS	Oxidative Stress
PCR	Polymerase Chain Reaction
PD	Parkinson's Disease
PKC	Protein Kinase C
pPD95.77	plasmid vector
pPK719	plasmid DNA carrying the coding sequence of the unc-119 gene
pRF4	plasmid DNA carrying the coding sequence of the mutant collagene rol-6(su1006) causing a dominant "roller" phenotype
RNAi	RNA interference or Post-Transcriptional Gene Silencing
ROS	Reactive Oxygen Speicies
sec	seconds
SEM	Standard Error of the Mean
SEpHluorin	Super-Ecliptic pHluorin, a pH sensitive GFP variant
SGK1	Serum and Glucocorticoid-induced protein Kinase 1
SLC5A11	sodium/SoLute Cotransporter-like 5A11
SVs	Synaptic Vesicles
TRP	Transient Receptor Potential
TVEC	Two-Electrode Voltage Clamp
UTRs	UnTranslated regions
w/v	weight per volume
wt	wild type
YFP	Yellow Fluorescent Protein
Δ	difference
ΔE_{rev}	reversal potential shift
μg	microgram
μl	microlitre
μm	micrometre
μM	microMolar

Table S2. List of *C. elegans* neurons referred in the paper, Related to Figure 1**.**

Neuron Name	Description	Neuronal type	Location	DELs expression
ADEL/R	Anterior DEirids Left/Right	mechanosensory, dopaminergic	head	DEL-3, DEL-4
ADF	Amphid neurons with Dual ciliated endings	sensory (gustatory, oxygen-sensory), serotonergic	head	
ASE	Amphid neurons with Single-ciliated Endings	gustatory, glutamatergic	head	DEL-2, DEL-3, DEL-4
ASH	Amphid neurons with Single-ciliated Endings	polymodal sensory, glutamatergic	head	DEL-2, DEL-4
ASI	Amphid neurons with Single-ciliated Endings	sensory (gustatory, thermosensory), insulin releasing	head	DEL-2 DEL-4
CEPDL/R	Dorsal Left/Right neurons of CEPhalic sensilla	mechanosensory, dopaminergic	head	DEL-2, DEL-3, DEL-4
CEPVL/R	Ventral Left/Right neurons of CEPhalic sensilla	mechanosensory, dopaminergic	head	DEL-3, DEL-4
DA 1-9	Ventral cord "dorsal A" motor neurons	motor, cholinergic	body (ventral nerve cord)	DEL-4
DB 1-7	Ventral cord "dorsal B " motor neurons	motor/proprioceptive, cholinergic	body (ventral nerve cord)	DEL-4
NSML/R	NeuroSecretory Motor neurons Left/Right	motor, sensory (proprioceptive/mechanosensory), serotonergic	pharynx (anterior bulb)	DEL-3, DEL-4
PDE	Posterior DEirid neurons	sensory, dopaminergic	posterior half of the body	DEL-3, DEL-4
PHA	PHAsmid neurons	chemosensory, glutamatergic	tail, right and left lumbar ganglia	DEL-2, DEL-3, DEL-4
PHB	PHasmid neurons	chemosensory, glutamatergic	tail, right and left lumbar ganglia	DEL-2, DEL-3
PHC	PHasmid neurons	thermosensory, glutamatergic	tail, right and left lumbar ganglia	DEL-2, DEL-3
PVM	Posterior Ventral Microtubule neuronal cell	mechanosensory	left side to the posterior half of the body	DEL-4
URX	head neurons with nonciliated dendritic endings	oxygen and minor CO_2 sensory, cholinergic	head	

VA 1-12	Ventral Cord motor neurons	motor, cholinergic	body (ventral nerve cord)	DEL-4
VB 1-11	Ventral Cord motor neurons	motor, proprioceptive	body (ventral nerve cord)	DEL-4
amphid	sensory organ consisting of 12 sensory neurons (ADF, ADL, AFD, ASE, ASG, ASH, ASI, ASJ, ASK, AWA, AWB, AWC) and one socket cell	sensory	head (posterior to the nerve ring)	
phasmid	sensory organ consisting of 3 sensory neurons (PHA, PHB, PQR), one sheath and two socket cells	sensory	tail (lateral sides, behind the rectum)	
deirid	a pair of sensory papillae		lateral cervical region	

**Information retreived form WORMATLAS (https://www.wormatlas.org/neurons/Individual%20Neurons/Neuronframeset.html)*

Table S3. List of genetic neuronal markers used in the paper, Related to Figure 1.

Neuronal Marker	Expression pattern	Type of Neurons
OSM-10::GFP	ASH, ASI, PHA, PHB	sensory, glutamatergic
p_{flp-8}GFP	ASE, URX, PVM, AUA, AVM	sensory
p_{dat-1}GFP	CEP, ADE, PDE	dopaminergic
TPH-1::GFP	NSM, ADF, HSN, AFD	serotonergic
p_{acr-2}GFP	VA/B, DA/B	motor, cholinergic
p_{unc-47}GFP	RME, AVL, RIS, DVB, VD, DD	motor, GABAergic
p_{unc129}NLP-21::Venus	DA/B, MC	motor, cholinergic

**Information retrieved form WORMBASE (https://wormbase.org/)*

Table S4. List of *C. elegans* genes referred in the paper and their mammalian orthologs, Related to Star methods.

***C. elegans* Gene**	**Definition of Nematode Gene**	**Human Ortholog**	**Definition of Human Ortholog**
aak-2	AMP-Activated Kinase	PRKAA1 and 2	PRotein Kinase AMP-activated catalytic subunit Alpha 1 and 2
acd-1	ACid-sensitive Degenerin	ASIC4	Acid Sensing Ion Channel subunit family member 4
acr-2	AcetylCholine Receptor	CHRNA3 and 6	CHolinergic Receptor Nicotinic Alpha 3 subunit and alpha 6 subunit
age-1	AGEing alteration	PIK3CB, D and G	PhosphatidylInositol-4,5-bisphosphate 3-Kinase Catalytic subunit Beta, Delta and Gamma
asic-1	Acid-Sensing/Amiloride-Sensitive Ion Channel	SCNN1B, D and G	sodium channel epithelial 1 subunit beta, delta and gamma
cat-2	abnormal CATecholamine distribution	TH	Tyrosine Hydroxylase
che-2	abnormal CHEmotaxis	IFT80	IntraFlagellar Transport 80
daf-16	abnormal DAuer Formation	FOXO4	FOrkhead boX O4
daf-2	abnormal DAuer Formation	IGF1R, INSR and INSRR	insulin-like growth factor 1 receptor, insulin receptor and insulin receptor related receptor
dat-1	DopAmine Transporter	SLC6A2 and 3	solute carrier family 6 member 2 and 3
del-2	DEgenerin Like		
del-3	DEgenerin Like		
del-4	DEgenerin Like	SCNN1G	sodium channel epithelial 1 subunit gamma
dop-1	DOPamine receptor	DRD1	dopamine receptor D1
dop-2	DOPamine receptor	DRD3	dopamine receptor D3
dop-3	DOPamine receptor	DRD3	dopamine receptor D3
flp-8	FMRF-Like Peptide		
goa-1	G protein,O, Alpha subunit	GNAO1	G protein subunit alpha o1
gst-4	Glutathione S-Transferase		
hsf-1	Heat Shock Factor	HSF1 and 2	heat shock transcription factor 1 and 2
hsp-16.2	Heat Shock Protein		
hsp-4	Heat Shock Protein	HSPA5	heat shock protein family A (Hsp70) member 5
kin-1	protein KINase	PRKACA	protein kinase cAMP-activated catalytic subunit alpha
kin-2	protein KINase	PRKAR1B	protein kinase cAMP-dependent type I regulatory subunit beta
let-858	LEThal	CWC22	spliceosome associated protein homolog
lin-15	abnormal cell LINeage		
myo-2	MYOsin heavy chain structural genes	MYH1, 2 and 3	myosin heavy chain 1, 2 and 3
myo-3	MYOsin heavy chain structural genes	MYH1, 2 and 3	myosin heavy chain 1
nlp-21	Neuropeptide-Like Protein		

osm-10	OSMotic avoidance abnormal		
pkc-1	Protein Kinase C	PRKCE	protein kinase C epsilon
pkc-2	Protein Kinase C	PRKCA	protein kinase C alpha and beta
pmp-3	Peroxisomal Membrane Prorein related	ABCD4	ATP binding cassette subfamily D member 4
rab-3	RAB family	RAB3A	member RAS oncogene family
rol-6	ROLler: helically twisted, animals roll when moving	COLQ	collagen like tail subunit of asymmetric acetylcholinesterase
skn-1	SKiNhead	NFE2, NFE2L1, NFE2L2	Erythroid Nuclear Factor 2, NFE2 like bZIP transcription factor 1 and 2
snb-1	SyNaptoBrevin related	VAMP2	vesicle associated membrane protein 2
snt-1	SyNapTotagmin	SYT1	synaptotagmin 1
sod-3	SuperOxide Dismutase	SOD2	superoxide dismutase 2
tpa-1	tetradecanoyl phorbol acetate resistant	PRKCD and PRKCQ	protein kinase C delta and protein kinase C theta
tph-1	TryPtophan Hydroxylase	TPH1 and 2	tryptophan hydroxylase 1 and 2
xbp-1	X-box Binding Protein	XBP1	X-box binding protein 1
unc-119	UNCoordinated	UNC-119	lipid binding chaperone
unc-129	UNCoordinated	GDF10	growth differentiation factor 10
unc-43	UNCoordinated	CAMK2D	(calcium/calmodulin dependent protein kinase II delta
unc-47	UNCoordinated	SLC32A1	solute carrier family 32 member 1
unc-49	UNCoordinated		
unc-54	UNCoordinated	MYH1, 2 and 3	myosin heavy chain 1, 2 and 3

**Information retrieved from WORMBASE (https://wormbase.org/)*